OPEN ACCESS Freely available online

PLOS | COMPUTATIONAL BIOLOGY

Membrane-Elasticity Model of Coatless Vesicle Budding Induced by ESCRT Complexes

Bartosz Różycki[1,2], Evzen Boura[3], James H. Hurley[3], Gerhard Hummer[1]*

1 Laboratory of Chemical Physics, National Institute of Diabetes and Digestive and Kidney Diseases, National Institutes of Health, Bethesda, Maryland, United States of America, **2** Max Planck Institute of Colloids and Interfaces, Department of Theory and Bio-Systems, Potsdam, Germany, **3** Laboratory of Molecular Biology, National Institute of Diabetes and Digestive and Kidney Diseases, National Institutes of Health, Bethesda, Maryland, United States of America

Abstract

The formation of vesicles is essential for many biological processes, in particular for the trafficking of membrane proteins within cells. The Endosomal Sorting Complex Required for Transport (ESCRT) directs membrane budding away from the cytosol. Unlike other vesicle formation pathways, the ESCRT-mediated budding occurs without a protein coat. Here, we propose a minimal model of ESCRT-induced vesicle budding. Our model is based on recent experimental observations from direct fluorescence microscopy imaging that show ESCRT proteins colocalized only in the neck region of membrane buds. The model, cast in the framework of membrane elasticity theory, reproduces the experimentally observed vesicle morphologies with physically meaningful parameters. In this parameter range, the minimum energy configurations of the membrane are coatless buds with ESCRTs localized in the bud neck, consistent with experiment. The minimum energy configurations agree with those seen in the fluorescence images, with respect to both bud shapes and ESCRT protein localization. On the basis of our model, we identify distinct mechanistic pathways for the ESCRT-mediated budding process. The bud size is determined by membrane material parameters, explaining the narrow yet different bud size distributions *in vitro* and *in vivo*. Our membrane elasticity model thus sheds light on the energetics and possible mechanisms of ESCRT-induced membrane budding.

Citation: Różycki B, Boura E, Hurley JH, Hummer G (2012) Membrane-Elasticity Model of Coatless Vesicle Budding Induced by ESCRT Complexes. PLoS Comput Biol 8(10): e1002736. doi:10.1371/journal.pcbi.1002736

Editor: Vijay S. Pande, Stanford University, United States of America

Received March 20, 2012; **Accepted** August 23, 2012; **Published** October 18, 2012

Funding: This research was supported by a Marie Curie International Outgoing Fellowship within the 7th European Community Framework Programme (B.R.), the Intramural AIDS Targeted Antiviral Program (J.H.H.), and the Intramural Research Program of the NIH, NIDDK (B.R., E.B., J.H.H., G.H.). The funders had no role in study design, data collection and analysis, decision to publish, or preparation of the manuscript.

Competing Interests: The authors have declared that no competing interests exist.

* E-mail: Gerhard.Hummer@nih.gov

Introduction

Lipid membranes enclose the cytosol of biological cells and compartmentalize their interior. The structure and contents of cellular membranes are actively controlled to sustain the vital functions of the cell. Transport vesicles are used to traffic membrane-bound proteins between cellular compartments. The best-characterized pathways of vesicle formation include those facilitated by BAR domain proteins [1] and by the coat protein clathrin with its adaptors [2]. Coat proteins impose their curved shape onto the membrane, thereby promoting vesicle curvature in an intuitively straightforward and computationally well-characterized process [3–5]. In the degradative transport of membrane proteins from endosomes to lysosomes (Fig. 1), small patches of the endosomal membrane bud into the interior (lumen) of the endosome and detach, forming intralumenal vesicles (ILVs) [6,7]. This pathway is catalyzed by the cytosolic Endosomal Sorting Complex Required for Transport (ESCRT) [8–10]. The ESCRT proteins are not internalized in ILVs, but rather recycled continuously in the cytosol [11,12]. To avoid the consumption of ESCRT proteins within the ILVs, these vesicles contain no protein coat to template their shape. Rather, these vesicles are initially formed as buds whose necks are stabilized by an assembly of ESCRT-I and -II [13]. As the assembly matures with the incorporation of ESCRT-III, the bud neck is cleaved from the cytosolic side, leaving ESCRTs in the cytosol and the detached spherical ILVs in the lumen of the endosome. Because this process involves no protein coat, the shape and energy of the mature buds must be governed primarily by membrane mechanical properties.

Until recently, the membrane remodeling functions of ESCRT were attributed only to ESCRT-III proteins, which assemble on liposomes *in vitro* [14], induce the ILV formation in giant unilamellar vesicles (GUVs) [12] and cause the plasma membrane to bud and tubulate when overexpressed in cells [15]. Based on these experimental observations, membrane deformations induced by ESCRT-III have been modeled [12] and studied theoretically [16]. An unresolved problem of these models was their inability to explain how the ESCRT-III proteins can be recycled from self-induced buds or tubes.

Recent *in vitro* experiments showed, however, that ESCRT-I and -II together are responsible for vesicle budding [13]. In these experiments, vesicle budding could be induced at physiological concentrations (15 nM) of ESCRT-I and -II. Fluorescence microscopy showed ESCRT-I and -II to be colocalized in the neck region of the buds (Fig. 1C), where they were shown to recruit ESCRT-III. The latter proteins then induced membrane scission [12]. Importantly, the ESCRT proteins were not found in the bud lumen. In this way, the ESCRT machinery that facilitates membrane budding and scission is not consumed in the process of ILV formation (Fig. 1D). Moreover, with ESCRT binding

Author Summary

Lipid membranes enclose the cytosol of biological cells and compartmentalize their interior. Vesicles are used to transport membrane proteins between cellular compartments. The ESCRT protein machinery induces the creation of such vesicles away from the cytosol. The resulting vesicles are uncoated by protein. Upon vesicle scission and release into the endosome, the ESCRT proteins are recycled into the cytosol. We develop a membrane-elasticity model that captures this budding process. The model reproduces the vesicle morphologies observed in fluorescence microscopy images, and identifies the energetic driving force of vesiculation. We also characterize possible mechanisms of ESCRT-induced membrane budding. The size of the resulting vesicles is determined by membrane material parameters, explaining the narrow yet different bud size distributions *in vitro* and *in vivo*. Our membrane elasticity model thus provides insight into the energetics and mechanisms of uncoated vesicle formation.

restricted to the neck region, the principal part of vesicle buds *in vitro* is thus bare lipid membrane.

Fluorescence microscopy [13] also showed that membrane-bound ESCRT proteins form microdomains on vesicle membranes (Fig. 1B and 1C). The lipid composition of these domains likely differs from that in the ESCRT-free membrane portions because ESCRTs bind specifically to certain charged lipids (PI3P) and could employ raft-favoring lipids and cholesterol to facilitate membrane budding [17,18].

These two experimental observations of (i) the formation of ESCRT microdomains on the membrane and (ii) the formation of coatless buds (with ESCRT proteins localized in the bud neck) jointly form the basis for a phenomenological model of ESCRT-induced budding. Observation (i) provides us with the starting point for the budding process and motivates a mechanism that can provide the large energy necessary for membrane deformation. Observation (ii) determines the end point of the budding pathway. In our model, we assume that the ESCRT-I-II supercomplexes have an enhanced affinity for binding to saddle-shaped membrane regions, and that a line tension acts on the outer boundary of an ESCRT-sequestered membrane domain. We cast our model in the framework of membrane elasticity theory. A bending elastic model of lipid bilayers was previously used to study the energetics of a possible mechanism of ESCRT-III induced fission of nascent vesicles [19]. Here we employ a similar approach to study the ESCRT-I-II induced formation of vesicle buds.

The analytical solutions of our model allow us to map out different membrane morphologies over a range of possible physical parameters. We identify a regime of membrane bending parameters and line tensions for which the minimum energy configurations are coatless membrane buds with ESCRTs localized in the bud neck. These minimum energy configurations closely resemble the fluorescence images observed in experiment [13]. Within our model, we also identify energetically and kinetically feasible budding pathways, and propose a three-stage mechanism of ESCRT-driven budding: (i) membrane-bound ESCRT-I-II complexes form clusters, or domains, and induce a line tension on the domain boundaries through local segregation of lipids; (ii) as the domain boundary energy exceeds a threshold level, the membrane patch sequestered by the ESCRT assemblies buckles and forms a bud; (iii) the ESCRT-I-II complexes scaffold the bud neck and thus stabilize a neck diameter optimized for ESCRT-III protein binding and bud scission. To validate the model, we compare its predictions for bud shapes, sizes, and formation kinetics to experiment [13,20]. We also relate our model to recent experiments probing ESCRT-induced lipid segregation in membranes [21].

Model

In the framework of membrane elasticity theory, the energy of membrane deformations consists of the mean curvature term

$$E_\kappa = \frac{\kappa}{2}\int_\Sigma \mathrm{d}A(C_1 + C_2 - C_0)^2 \tag{1}$$

and the Gaussian curvature term

$$E_G = \bar{\kappa}\int_\Sigma \mathrm{d}A C_1 C_2 \tag{2}$$

where κ and $\bar{\kappa}$ are the mean and Gaussian bending rigidity moduli, respectively; C_1 and C_2 are the principal local curvatures; C_0 is the spontaneous curvature; and the integrals are performed over the membrane surface Σ [22]. For uniform membranes with fixed topology, the energy term E_G does not depend on membrane shape. Consistent with *in vitro* experiments [13], we will consider symmetric lipid bilayers with no spontaneous curvature, $C_0 = 0$.

Eq. (1) implies that the energetic cost of forming a vesicle bud [23–27] is approximately $8\pi\kappa$, which exceeds $100 k_B T$ for typical membrane bending rigidities $\kappa \sim 10 k_B T$. This large energetic cost effectively eliminates random thermal fluctuations as a main factor. Instead, the energetic cost of the nascent vesicle bud has to be offset by the molecular machinery that drives the budding process. In ESCRT-induced budding, the source of this offset energy is provided by the binding of the ESCRT proteins to the membrane. But unlike BAR domains or clathrin proteins, the ESCRT machinery does not seem to use the scaffold mechanism as the primary mode of action. Indeed, the scaffold mechanism cannot easily account for the significantly different bud radii *in vitro* ($R_{\mathrm{bud}} \approx 1\mu\mathrm{m}$ [13]) and *in vivo* ($R_{\mathrm{bud}} \approx 25\mathrm{nm}$ [20]), and appears to be contradicted by the experimental observation that the ESCRT proteins colocalize in the neck of buds.

How does the ESCRT machinery deform a flat membrane patch into a bud [28]? There are two relevant observations that help answer this question. Firstly, there is increasing evidence that the insertion of amphipathic, cationic peptide segments into the lipid bilayer can induce negative Gaussian curvature [29–31], which is a characteristic of the bud necks where the ESCRT proteins localize. The Vps37 subunit of ESCRT-I has such a cationic helix at its N-terminus [32], as does the Vps22 subunit of ESCRT-II [33]. It is therefore possible that the ESCRT-I-II proteins generate negative Gaussian curvature by inserting amphipathic and cationic segments into the membrane. In the lowest order of approximation, the resulting curvature-dependent binding energy,

$$E_\epsilon = \epsilon\int_{\Sigma_0} \mathrm{d}A C_1 C_2, \tag{3}$$

is proportional to the membrane Gaussian curvature $C_1 C_2$ integrated over an ESCRT-rich membrane patch Σ_0, where ϵ is a coupling constant. Remarkably, we also arrive at an energy term that is formally equivalent to Eq. (3) on an entirely different route. If we assume that by binding to the membrane, the ESCRT-I-II proteins locally perturb its Gaussian bending modulus according

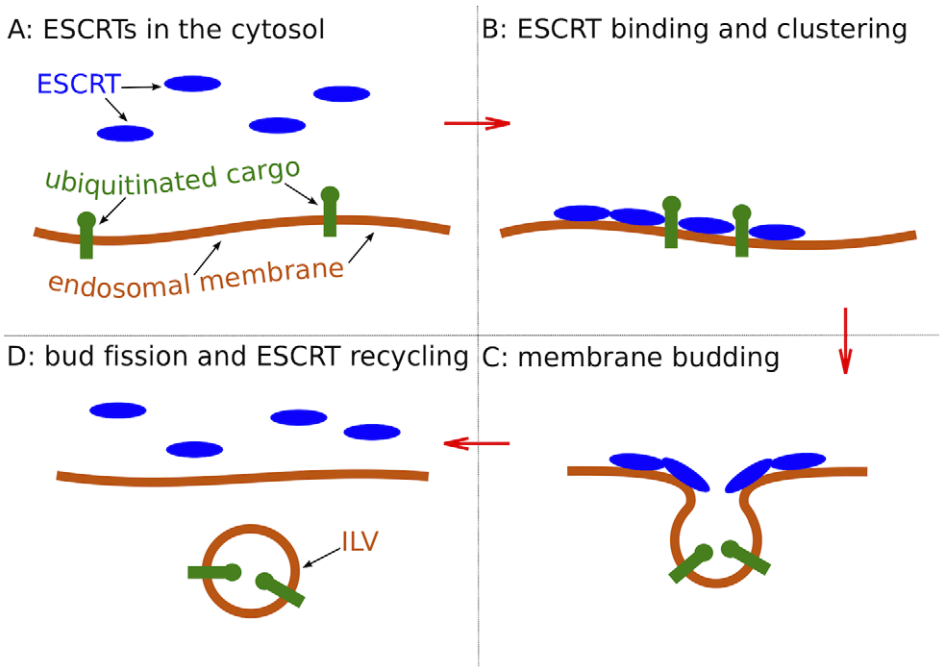

Figure 1. ESCRT protein assemblies (blue) facilitate the sorting of ubiquitinated membrane proteins (green) and formation of intralumenal vesicles (ILV). The ESCRT proteins assemble on the membrane side opposite the vesicle bud (C) and do not enter the ILV lumen for possible recycling (D). Energy input from ATP hydrolysis accelerates disassembly of the ESCRT machinery (D), but is not required in steps (A–C).
doi:10.1371/journal.pcbi.1002736.g001

to Eq. (2), then the parameter ϵ can be understood as the Gaussian bending modulus contrast $\delta\bar{\kappa}$. The energy term in Eq. (3) thus accounts for both the preferential binding to saddle-shaped features of the membrane and for changes in the Gaussian bending modulus in response to binding, with different interpretations of the constant ϵ.

The second relevant observation is that late endosomes contain raft-like domains that are rich in cholesterol and sphingomyelin [34–36]. The *in vitro* experiments [13] were performed on vesicles containing cholesterol, raft-favoring lipids and PI3P, which is consistent with the possibility that ESCRTs could use lipid rafts or domains to promote membrane budding [17,18]. The ESCRT proteins could bind to pre-existing rafts or induce lipid domain formation. In fact, proteins with multiple lipid binding sites can induce lipid segregation in membranes close to the demixing point [37–40]. Lipid segregation has been suggested as a factor driving scission in endocytosis [41]. The enhancement of lipid segregation upon protein binding is primarily an entropic effect. Lipid segregation has to overcome an entropic penalty to move away from a perfectly mixed state. This penalty is reduced by concentrating certain lipids through preferential binding because the entropic cost of rearranging the resulting clusters of protein-bound lipids is smaller than that of rearranging individual lipids.

We consider a single lipid-segregated domain Σ. A line tension λ acts on the boundary $\partial\Sigma$ of this domain, where the corresponding energy is proportional to the length of the boundary line

$$E_\lambda = \lambda \int_{\partial\Sigma} \mathrm{d}l. \tag{4}$$

To quantify the preferential binding of ESCRTs to lipid rafts or domains, we introduce an additional energy term in the spirit of mean field theory

$$E_\mu = -\mu \int_{\Sigma\cap\Sigma_0} \mathrm{d}A. \tag{5}$$

Here, μ is an effective ESCRT binding free energy per unit area, and $\Sigma\cap\Sigma_0$ denotes the intersection of the lipid-segregated domain Σ and the ESCRT-rich domain Σ_0 on the membrane, where we assume that the latter is a subset of the former, $\Sigma_0 \subset \Sigma$. In the following, we assume the shapes of Σ and Σ_0 to be circular and ring-shaped, respectively.

As we show below, a minimal model of ESCRT proteins inducing or enhancing lipid segregation can explain central experimental results, in particular the narrow yet different bud-size distributions *in vivo* and *in vitro*. Moreover, the line tension on the boundaries of the lipid-segregated membrane domains [42–44] can also provide the large energetic driving force for vesicle budding [45–48].

Our model is defined by the energy functional

$$E = E_\kappa + E_\epsilon + E_\lambda + E_\mu, \tag{6}$$

which combines the energy terms in Eqs. (1), (3), (4), and (5). The four corresponding parameters κ, ϵ, λ, and μ depend on membrane lipid composition, on external conditions such as temperature, and on ESCRT molecular properties, which are not entirely understood yet. Therefore, the model parameters can take different values depending on the molecular details of the ESCRT-membrane system. We thus use the spherical cap approximation [45,49] to derive analytical solutions that allow us to map out the entire parameter space of the model. We then minimize the energy functional Eq. (6) with respect to the membrane shape and the ESCRT cluster location, and investigate the membrane states, or morphologies, that are stable in different parameter regimes.

Interestingly, we find a range of physically meaningful parameters in which the minimum energy states closely resemble the fluorescence images in Ref. [13]. We also investigate possible budding pathways that lead without activation barriers from a flat membrane state to the coatless membrane bud with ESCRTs localized in the neck.

Results

In the following, we first develop an approximate analytic treatment that accurately captures the energetics. We then report the results of numerical calculations that allow us to test the analytical solutions and to provide detailed information about the bud shapes. Finally, we analyze possible budding pathways.

Energetics and morphology diagrams

To make our model analytically tractable, we applied the spherical cap approximation, which is known to capture the energetics of unassisted membrane budding [45,49]. In the spherical cap approximation, the energy functional Eq. (6) becomes a simple function whose minima can be found analytically (see Methods). The phase diagram that results from the energy minimization for $\epsilon<2\kappa$ displays three regimes which are shown in Fig. 2. For small line tensions λ (left side of Fig. 2), the membrane resists bending and remains flat. The lipid-segregated domain Σ and the ESCRT-rich domain Σ_0 colocalize entirely. For large line tensions λ and large binding energies μ (top right corner of Fig. 2), the membrane buckles and forms an ESCRT-covered bud. Again Σ and Σ_0 colocalize. For large λ and small μ (bottom right corner of Fig. 2), the minimum energy configurations are coatless buds with ESCRTs localized in the bud neck.

Membrane shape

To test the spherical cap approximation and to calculate bud shapes, we minimized the energy functional Eq. (6) numerically

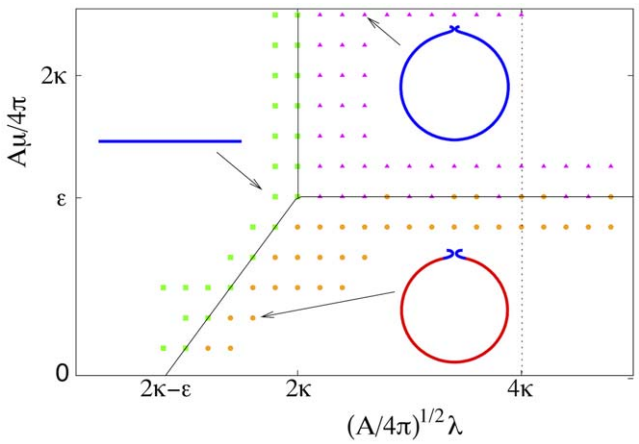

Figure 2. Membrane morphology diagram from the analytical solution obtained for the spherical cap approximation (lines) and from numerical energy minimizations (symbols). Results are shown for a Gaussian bending modulus fixed at $\epsilon=1.2\kappa$. The green squares represent the flat membrane state. The magenta triangles correspond to ESCRT-coated membrane buds. The orange circles represent bare lipid buds with ESCRTs localized in the bud neck. The black solid lines are the coexistence lines, and the black dotted line represents the spinodal at which the energetic barrier to bud formation vanishes. Exemplary membrane shapes are shown for indicated points. The red and blue lines represent lipid domains and ESCRT-rich domains, respectively.
doi:10.1371/journal.pcbi.1002736.g002

with respect to the membrane shape and the location of the ESCRT cluster (see Methods). To distinguish different morphologies of the minimum energy configurations, we introduced the area fraction $y=(A-A_0)/A$, where A and A_0 denote the areas of the lipid segregated domain Σ and the ESCRT-rich domain Σ_0, respectively. We grouped all the minimum energy configurations found numerically into three distinct categories: (i) flat membrane domains with zero bending energy and area fraction $y=0$, (ii) ESCRT-coated buds with bending energy $E_\kappa\approx 8\pi\kappa$ and area fraction $y>0.6$, and (iii) coatless buds with $E_\kappa\approx 8\pi\kappa$, small area fraction $y<0.3$, and the ESCRT cluster located primarily in the bud neck region. The resulting morphology diagram agrees very well with the diagram based on the spherical cap approximation (Fig. 2).

The spherical cap model predicts discontinuous transitions between the different morphological phases, with a kink in the minimum energy at the transition lines. In the complete model, however, the kink is rounded at the transition line $\mu A=4\pi\epsilon$ due to the finite-size of the bud neck (Fig. 3A).

To additionally quantify the bud morphologies, we determined the tangent angle $\phi_0=\Psi(s_2)$ (see Methods) along the longitude at the boundary of the ESCRT-coated domain. The angle ϕ_0 as well as the area fraction y exhibit an abrupt change at the transition line $\mu A=4\pi\epsilon$, as shown in Fig. 3, which further justifies the distinction between ESCRT-coated buds and uncoated buds.

It is instructive to have a closer look at the membrane buds shown in the bottom right corner of Fig. 2. The principal part of these buds is coatless membrane, and the ESCRT cluster is localized only in the bud neck. These coatless buds assume the shape of a sphere. The geometry of the bud neck follows that of a catenoid, a minimal surface with no mean curvature, $C_1+C_2=0$, and thus zero bending energy [24–27]. As a result, the bending energy of the buds approaches the bending energy of a spherical vesicle, $8\pi\kappa$. We note that our calculated bud shapes, as shown in the top right corner of Fig. 2, resemble the tomographic images of early endosomes [20] and the fluorescence images of GUV buds observed *in vitro* [13].

Budding mechanisms

Within the framework of the spherical cap approximation, we also analyzed possible budding pathways. We focused in particular on activation-less pathways along which the buds grow without having to cross significant energy barriers (see Methods). This analysis revealed a three-stage mechanism of ESCRT-mediated membrane budding. In stage (i) the ESCRT-rich domain Σ_0 and the lipid-segregated domain Σ colocalize entirely on the flat membrane if $\epsilon<2\kappa$. As the domain radius increases beyond $R_*=4\kappa/\lambda$, the energy of the flat domain becomes larger than the energy of an ESCRT-covered bud. As the domain radius increases to $R_+=8\kappa/\lambda$, the barrier between these membrane states vanishes entirely and the system enters into stage (ii) in which the flat membrane domain buckles and forms an ESCRT-covered bud. The resulting bud has a radius

$$R_b=R_+/2=4\kappa/\lambda, \tag{7}$$

which, interestingly, is determined by membrane material parameters. In stage (iii) the ESCRTs coalesce into the bud neck with no energy barriers if $\epsilon>16\kappa^2\mu/\lambda^2$. The third stage is driven by the energy ϵ of the ESCRT preferential binding to membrane regions with negative Gaussian curvature. Importantly, in stage (iii), the bud is cleared of ESCRTs for possible recycling.

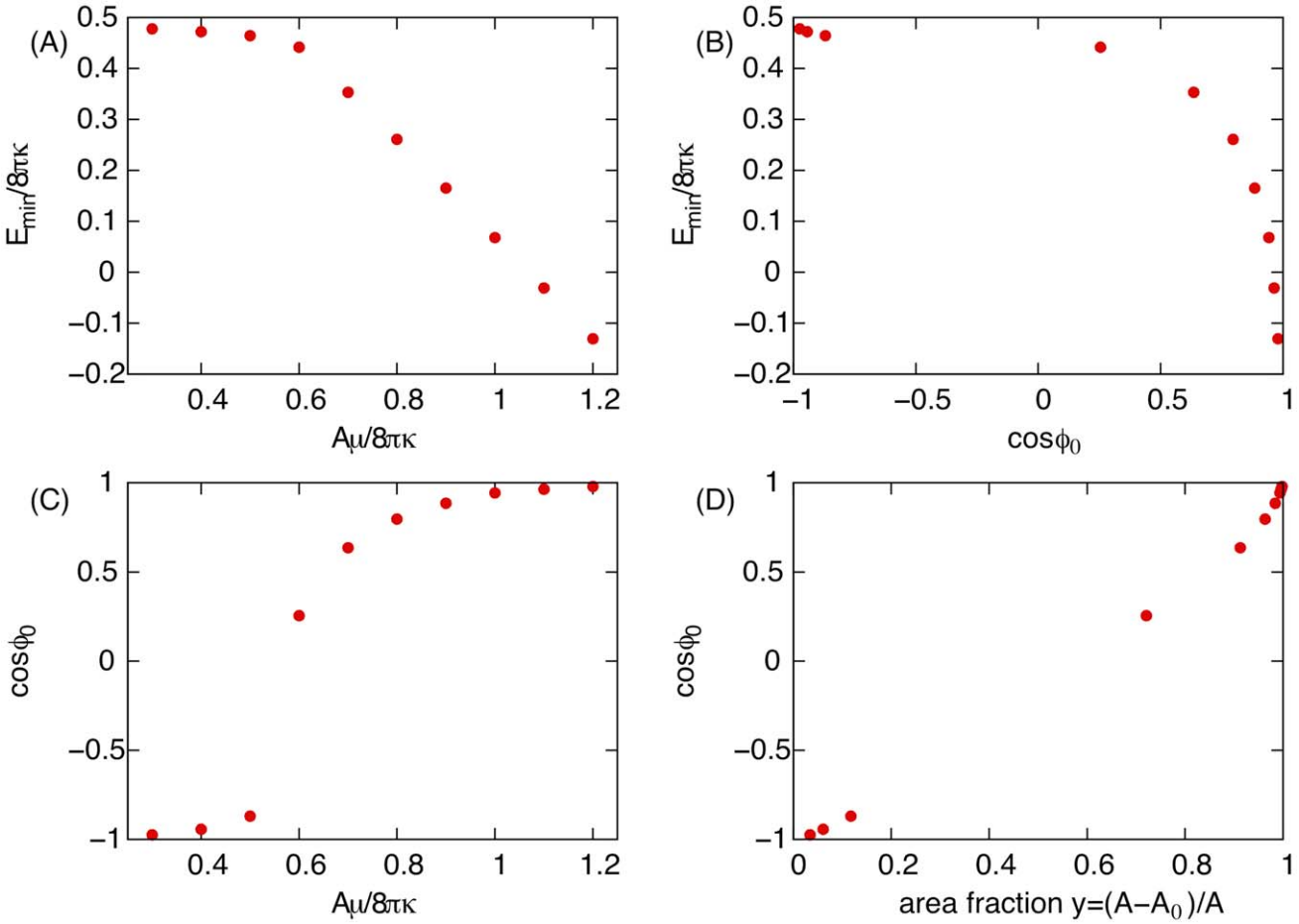

Figure 3. Relation between energetic and geometric properties, obtained by numerical minimization of the energy functional Eq. (6) for fixed parameters $\epsilon = 1.2\kappa$ and $(A/4\pi)^{1/2}\lambda/2\kappa = 1.2$. (A) Minimum energy $E_{\min}$ rescaled by the membrane bending rigidity κ as a function of the ESCRT binding energy μ rescaled by the area A of the lipid-segregated domain. (B) Minimum energy $E_{\min}$ as a function of the cosine of the membrane tangent angle ϕ_0 along the lines of longitude at the boundary of the ESCRT-coated domain. (C) $\cos\phi_0$ as a function of the binding energy μ rescaled by the area A of the lipid-segregated domain Σ. (D) $\cos\phi_0$ as a function of the area fraction $y=(A-A_0)/A$, where A_0 is the area of the ESCRT-rich domain Σ_0.
doi:10.1371/journal.pcbi.1002736.g003

If $\epsilon > 2\kappa$, the mechanism of ESCRT-mediated membrane budding is different. The flat membrane with ESCRTs bound is then unstable and the system evolves spontaneously to a transient state, in which ESCRT-free buds with radius $R_b \to 0$ are formed. The mini-buds, induced by a strong binding preference ϵ to saddle-shaped membrane structures, are next squeezed bigger by line tension λ if the radius of the ESCRT-coated membrane patch is smaller than λ/μ. The latter condition puts an upper bound on the ESCRT-free bud radius $R_b < \lambda/2\mu$. Interestingly, on this budding pathway the ESCRTs never coat the bud. We note, however, that this pathway is somewhat problematic since the linear approximation in Eq. (3) may not be applicable for large parameters $\epsilon > 2\kappa$. In addition, effects of finite membrane thickness cannot be ignored in this regime.

Discussion

The detailed physical mechanisms used by the ESCRT machinery to control membrane budding are currently unknown. This lack of knowledge has motivated us to consider a simple, phenomenological model for ESCRT-induced membrane budding. Our model is based on well-established physical principles to ensure robustness. Following earlier studies of membrane tubulation [16] and fission [19] driven by ESCRT-III proteins, we have cast our model in the framework of membrane elasticity theory. The key assumption in our model is that ESCRTs induce or enhance the formation of raft-like domains in lipid membranes. Indeed, recent total internal reflection fluorescence (TIRF) images show that the ESCRT-II proteins induce lipid phase separation in model membranes with endosome-like composition [21]. These direct experimental observations thus support a central element of our theoretical model. However, to test and further quantitate our model will require additional studies of ESCRT-membrane interactions. In particular, line tension measurements would provide critical input in building a fully quantitative description of the budding process. In addition, studies of the different components of the ESCRT system, including modifications such as Vps20 myristoylation, should provide further guidance at which stage and to what extent lipid phase separation is induced. The TIRF experiments [21] indicate interesting variations, with the yeast ESCRT-II protein complex forming somewhat smaller and more numerous clusters than the human ESCRT-II protein complex under the same conditions. Ultimately, it will be important to determine if membrane curvature is induced in a

way consistent with our theoretical analysis. Such measurements would provide critical tests to what extent our model captures ESCRT-induced budding, and would help in its quantitation and refinement.

The energetic analysis of our model suggests a three-stage mechanism of vesicle budding induced by the ESCRT proteins. In the first stage, the ESCRT-I-II binding induces lipid phase segregation, consistent with the TIRF experiments [21]. We speculate that in this stage, ESCRT-I-II complexes loosely assemble on the membrane to form clusters or domains. The ESCRT-membrane interactions enhance lipid segregation in the membrane and induce a line tension λ on the domain boundaries. Once the lipid-segregated membrane domain exceeds a critical size, as determined by membrane material parameters according to our model, the process enters the second stage. Beyond a size threshold set by the ratio κ/λ, the energy barrier to membrane shape deformation disappears, and the membrane patch sequestered by ESCRTs buckles and forms a bud. In the third stage, according to our energy function, the ESCRT-I-II complexes concentrate in the neck of the newly formed bud. This final step is driven the ESCRT binding energy ϵ to the membrane portions with negative Gaussian curvature. While our model lacks molecular detail of this curvature-dependent binding, recent experiments [29–31] suggest possible mechanisms. In particular, it could be caused by the insertion of amphipathic and cationic segments of the membrane-bound ESCRT proteins into the membrane, or by the formation of an assembly whose shape is complementary to that of the bud neck [50]. The formation of neck-coating assemblies by the ESCRT-I-II complexes not only would help recruit ESCRT-III proteins for scission, but could also clear the ESCRT-I-II proteins from the bud lumen and set them up for recycling.

The third stage of the budding process described above is dynamically feasible within the overall time scale of the process. The diffusion coefficient of membrane proteins is of order $1\mu\mathrm{m}^2/\mathrm{s}$ [51]. Provided a gradient to the bud neck region, the process of clearing *in vitro* buds with radius $R_\mathrm{b}\approx 1\mu\mathrm{m}$ [13] would be completed within $\sim 10\mathrm{s}$. The clearing process would be two orders of magnitude faster for the *in vivo* buds with radius $R_\mathrm{b}\approx 25\mathrm{nm}$ [20].

One immediate consequence of the three-stage mechanism is that the complete buds have a radius $R_\mathrm{b}=4\kappa/\lambda$ that is determined by membrane material parameters, namely membrane rigidity κ and line tension λ. Therefore, the bud radius R_b attains a particular value for a vesicle at given conditions, which explains the narrow distribution of bud sizes observed both *in vitro* [20] and *in vivo* [13]. We note, however, that both the line tension λ and the bending rigidity κ may be affected by details of the ESCRT-membrane interactions, which could explain small ILV size variations in response to mutations [52].

Despite the 40-times smaller radius R_b, the *in vivo* buds have the same bending energies and shapes as the buds observed *in vitro*. This conclusion is a direct consequence of the scale invariance of the membrane bending energy Eq. (1). However, the line tensions necessary to induce vesicle budding, $\lambda=4\kappa/R_\mathrm{b}$, are different. For *in vivo* buds with radius $R_\mathrm{b}\approx 25\mathrm{nm}$ and bending rigidity $\kappa\approx 5k_BT$ [53], we estimate $\lambda\approx 6\mathrm{pN}$; for *in vitro* buds with $R_\mathrm{b}\approx 1\mu\mathrm{m}$, we get $\lambda\approx 0.15\mathrm{pN}$ assuming the same membrane rigidity κ. Line tensions in this range have been measured in GUVs [42,47].

We note that the bending rigidity of early endosomes [53] is an order of magnitude lower than the bending rigidity of lipid membranes in the liquid-ordered phase [47,54]. This difference in mechanical properties may be caused by variations in the composition and by the presence and activity of proteins in the membrane of endosomes. The membrane-sculpting protein Sar1 of the COPII complex, for example, has been shown to lower the membrane rigidity below $\kappa=5k_BT$ [55]. The rigidity of fluid membranes has also been shown to decrease gradually with increasing concentration of the HIV-1 fusion peptide in the bilayer [56].

The three-stage budding process discussed above occurs if the Gaussian bending modulus contrast ϵ is limited to a window $2\kappa>\epsilon>16\kappa^2\mu/\lambda^2$. This relation puts an upper bound on the binding energy $\mu<\lambda^2/8\kappa$. For typical bending rigidities $\kappa\approx 5k_BT$ and line tensions $\lambda\approx 1\mathrm{pN}$, the required energy μ is of order k_BT per $500\mathrm{nm}^2$ or smaller.

If the affinity of ESCRTs to regions with negative Gaussian curvature is high, $\epsilon>2\kappa$, our model predicts a different budding pathway. In this case, flat ESCRT-coated membrane domains are unstable, and small ESCRT-free buds form spontaneously. The mini-buds induced by a strong binding preference ϵ to saddle-like membrane shapes can next be squeezed bigger by line tension λ. The latter transition occurs if the radius of the ESCRT-coated domain does not exceed λ/μ. The resulting ESCRT-free buds have a radius $R_\mathrm{b}<\lambda/2\mu$. For $\lambda\approx 1\mathrm{pN}$ and $\mu\approx 0.002k_BT/\mathrm{nm}^2$ as above, we get the bud radius R_b smaller than approximately $80\mathrm{nm}$, which is consistent with the size of late endosome buds, $R_\mathrm{b}\approx 25\mathrm{nm}$ [20].

In contrast to the three-stage mechanism, in the pathway starting with mini-buds the ESCRTs never enter the bud lumen. It is thus tempting to picture this alternative budding route as follows: ESCRT-0 and -I bind to the membrane with $\epsilon<2\kappa$ and the membrane remains flat. When ESCRT-II proteins bind to ESCRT-I and to the membrane, ϵ becomes larger than 2κ and the ESCRT-free membrane buds are formed spontaneously. The condition for forming a finite-size, ESCRT-free bud is that the radius of the ESCRT patch at the ESCRT-II arrival can not exceed $\lambda/\mu\approx 150\mathrm{nm}$. We notice, however, that this pathway might be an artifact of our model since the linear approximation in Eq. (3) could be inapplicable for large $\epsilon>2\kappa$. Nevertheless, we cannot entirely exclude this alternative pathway.

Overall, we favor the three-stage mechanism as a possible route for ESCRT-induced budding. It concisely explains the uniform bud sizes seen in experiment, and makes quantitative and testable predictions for their dependence on physical parameters. In particular, according to Eq. (7) the vesicle bud radius R_b should increase linearly as a function of the ratio κ/λ. Since the line tension λ depends sensitively on temperature [42], it should be possible to test this theoretical prediction in future experiments on GUVs.

A key element of the model is the Gaussian bending energy E_ϵ. Because of experimental difficulties, our understanding of Gaussian curvature effects is rather limited. However, factors affecting the Gaussian bending modulus [57,58] or enhancing the binding to membranes with negative Gaussian curvature [29–31] have been established. As detailed structural models of the full-length ESCRT protein supercomplexes emerge [50,59], it will be important to identify the interactions responsible for the preferential association of the ESCRT proteins to saddle-shaped bud-neck membrane regions. It may also be possible to study binding of ESCRT proteins or protein fragments to model systems with negatively curved membranes [29–31]. In this way, one could gain a microscopic quantification of the parameter ϵ, putting it on similar footing as the other membrane-bending terms.

Methods

We consider only axisymmetric vesicle buds as the lowest energy shape by symmetry. Their surface is described in terms of two parameters, the angle γ of rotation around the axis of symmetry, and the arc length s along longitudes. The vesicle bud surface then has Cartesian coordinates $X=R(s)\cos\gamma$, $Y=R(s)\sin\gamma$ and

$Z=Z(s)$, where $0\le\gamma\le 2\pi$ and $0\le s\le s_1$ and R is the distance from the Z-axis, which is the axis of symmetry of the bud. One can introduce a tangent angle Ψ such that $dR/ds=\cos\Psi(s)$ and $dZ/ds=\sin\Psi(s)$. In this parametrization, the principal local curvatures are $C_1=d\Psi/ds$ and $C_2=\sin\Psi/R$ [60,61]. Therefore, in this parametrization, Eq. (1) reads

$$E_\kappa=\pi\kappa\int_0^{s_1}\mathrm{d}sR(s)\left(\frac{d\Psi}{ds}+\frac{\sin\Psi(s)}{R(s)}\right)^2. \tag{8}$$

The lower limit of integration, $s=0$, corresponds to the "south pole" of the vesicle bud at which $\Psi(s=0)=R(s=0)=Z(s=0)=0$. With these boundary conditions we have $R(s)=\int_0^s\cos\Psi(s')\mathrm{d}s'$ and $Z(s)=\int_0^s\sin\Psi(s')\mathrm{d}s'$. The upper limit of integration in Eq. (8), $s=s_1$, corresponds to the bud rim, where $\Psi(s_1)=0$ and $R(s_1)=R_1$ to connect the bud smoothly to a flat membrane at a distance R_1 from the axis.

The boundaries of the ESCRT-occupied membrane patch are located at $s=s_2$ and $s=s_3$ with $0\le s_2<s_3\le s_1$. Eq. (3) takes the following form in the arc-length parametrization,

$$E_\epsilon=2\pi\epsilon\int_{s_2}^{s_3}R(r)\frac{d\Psi}{ds}\frac{\sin\Psi(s)}{R(s)}\mathrm{d}s, \tag{9}$$

which simplifies to

$$E_\epsilon=2\pi\epsilon(\cos\Psi(s_2)-\cos\Psi(s_3)). \tag{10}$$

In this parameterization, the energy terms in Eqs. (4) and (5) become

$$E_\lambda=2\pi\lambda R(s_1) \tag{11}$$

and

$$E_\mu=-2\pi\mu\int_{s_2}^{s_3}R(s)\mathrm{d}s. \tag{12}$$

The total energy is $E=E_\kappa+E_\epsilon+E_\mu+E_\lambda$.

Numerical calculations

It is convenient to use dimensionless variables in numerical calculations. Here we introduce

$$r(\tau)=R(s)/s_1,\quad z(\tau)=Z(s)/s_1,\quad \psi(\tau)=\Psi(s) \tag{13}$$

and $\tau=s/s_1$ with $\tau\in[0,1]$. With these dimensionless variables, the boundaries of the ESCRT-occupied membrane patch are described by parameters τ_2 and τ_3, where $0\le\tau_2<\tau_3\le 1$. The energy functional

$$\begin{aligned}\frac{E[\psi(\tau)]}{8\pi\kappa}&=\frac{1}{8}\int_0^1 r(\tau)\left(\frac{d\psi}{d\tau}+\frac{\sin\psi(\tau)}{r(\tau)}\right)^2\mathrm{d}\tau\\&+\tilde{\lambda}r(1)\left(2\int_0^1 r(\tau)\mathrm{d}\tau\right)^{-1/2}\\&-\tilde{\mu}\left(\int_{\tau_2}^{\tau_3}r(\tau)\mathrm{d}\tau\right)\left(\int_0^1 r(\tau)\mathrm{d}\tau\right)^{-1}\\&-\frac{\tilde{\epsilon}}{2}(\cos\psi(\tau_3)-\cos\psi(\tau_2))\end{aligned} \tag{14}$$

depends then on the bud shape, which is described by

$$\left\{\psi(\tau),r(\tau)=\int_0^\tau\cos\psi(\tau')\mathrm{d}\tau',z(\tau)=\int_0^\tau\sin\psi(\tau')\mathrm{d}\tau'\right\}; \tag{15}$$

on the domain location as given by τ_2 and τ_3; and on three dimensionless parameters

$$\tilde{\lambda}=\frac{\lambda}{2\kappa}\sqrt{\frac{A}{4\pi}}, \tag{16}$$

$$\tilde{\mu}=\frac{\mu}{2\kappa}\frac{A}{4\pi}, \tag{17}$$

and

$$\tilde{\epsilon}=\frac{\epsilon}{2\kappa}. \tag{18}$$

In deriving the equations above we used a relation between the contour length s_1 and the membrane area A, namely

$$A=2\pi\int_0^{s_1}R(s)\mathrm{d}s=2\pi s_1^2\int_0^1 r(\tau)\mathrm{d}\tau. \tag{19}$$

The membrane energy (14) is minimized numerically with respect to the bud shape $\psi(\tau)$ and the domain boundaries τ_2 and τ_3 using a simulated annealing method. To this end, the function $\psi(\tau)$ is assumed to be smooth at $\tau\in[0,1]$ and approximated by a Fourier series

$$\psi(\tau)=\sum_{n=1}^{N}a_n\sin(n\pi\tau) \tag{20}$$

that fulfills the boundary conditions $\psi(\tau=0)=0$ and $\psi(\tau=1)=0$. Here, N is the number of Fourier amplitudes a_n. In simulated annealing Monte Carlo moves, the amplitudes a_n and the boundary positions τ_2 and τ_3 are varied. We performed the numerical calculations with up to $N=100$ Fourier modes as in [62,63]. For any set of parameters $\tilde{\lambda}$, $\tilde{\mu}$, and $\tilde{\epsilon}$, numerical calculations were repeated twice with different initial configurations to ensure convergence to the global minimum.

Spherical cap approximation

To make our model analytically tractable, we approximate the nascent membrane bud by a spherical cap of radius R_b with a budding angle ϕ. A convenient budding coordinate is $x=(1-\cos\phi)/2$. We also define the area ratio $y=(A-A_0)/A$ where A and A_0 denote the areas of the lipid-segregated domain Σ and the ESCRT-rich domain Σ_0, respectively. The domain of the two dimensionless parameters x and y is the unit square. In the following, we write the energy of the bud in terms of x and y, considering two cases:

Case I: The whole lipid-segregated domain Σ forms a spherical cap and thus the membrane surface parametrization is given by $\Psi(s)=s/R_\mathrm{b}$ for $0\le s\le s_1$ with $s_1=\phi R_\mathrm{b}$. Then $A=4\pi R_\mathrm{b}^2x$ and the energy functional Eq. (6) becomes a two-variable function

$$E_\mathrm{I}(x,y)/8\pi\kappa=x-\tilde{\epsilon}xy+\tilde{\lambda}\sqrt{1-x}-\tilde{\mu}(1-y). \tag{21}$$

Case II: Only the ESCRT-free membrane patch forms a bud and therefore the membrane surface parametrization is given by

$\Psi(s)=s/R_b$ for $0\le s<s_2$ and $\Psi(s)=0$ for $s_2\le s\le s_1$ with $s_2=\phi R_b$. Then $A=A_0+4\pi R_b^2 x$ and

$$E_{II}(x,y)/8\pi\kappa = x-\tilde{\epsilon}x+\tilde{\lambda}\sqrt{1-xy}-\tilde{\mu}(1-y). \qquad (22)$$

In both cases I and II, the determinant of the 2×2 Hessian matrix is always negative within the unit square $0\le x\le 1$, $0\le y\le 1$, which implies that the local minima of $E(x,y)$ can be found only at the square boundaries. A simple analysis of Eqs. (21) and (22) shows that the local minima of the energy function are located only at the corners of the unit square in the $x-y$ plane. First, $E_I(0,0)/8\pi\kappa = E_{II}(0,0)/8\pi\kappa = \tilde{\lambda}-\tilde{\mu}$. Second, $E_I(1,0)/8\pi\kappa = 1-\tilde{\mu}$, and $E_{II}(1,0)/8\pi\kappa = 1-\tilde{\epsilon}+\tilde{\lambda}-\tilde{\mu}$. Third, $E_I(1,1)/8\pi\kappa = E_{II}(1,1)/8\pi\kappa = 1-\tilde{\epsilon}$. We compare these energies to find the global minimum of the energy function and, in this way, construct the phase diagram in Fig. 2.

Point (0,0) corresponds to the flat membrane state, which is obviously the starting point of the budding process. Point (1,0) on energy surface E_I corresponds to an ESCRT-coated bud, whereas point (1,0) on energy surface E_{II} corresponds to coatless buds with radius $R_b\to 0$. Point (1,1) corresponds to a coatless membrane bud with finite radius and ESCRTs localized in the neck. Fluorescence microscopy shows that this state is the end point of the ESCRT-induced budding.

The transition from the initial, flat membrane state at point (0,0) to the end point at (1,1) occurs spontaneously with no energy barriers if either (i) $\tilde{\lambda}>2$ and $\tilde{\lambda}>2\tilde{\epsilon}>2\tilde{\mu}$, or (ii) $\tilde{\epsilon}>1$ and $2\tilde{\epsilon}>\tilde{\lambda}>2\tilde{\mu}$. In case (i), the transition occurs on energy surface E_I. In case (ii), the system evolves on energy surface E_{II}. In both cases (i) and (ii) the transitions occur from point (0,0) to (1,0) along the $y=0$ line and next from point (1,0) to (1,1) along the $x=1$ line. We checked that for some parameter combinations, a saddle point can emerge within the unit square, separating local minima at (0,0) and (1,1). However, if the saddle point is in the unit square, it is higher than $E(0,0)$. We also checked that for positive parameters $\tilde{\lambda},\tilde{\epsilon}$ and $\tilde{\mu}$, the saddle point cannot merge with point (0,0). So the barrier-free path should indeed go from point (0,0) to (1,0) to (1,1).

In the case $\epsilon<2\kappa$, the system stays on energy surface E_I. It is then instructive to analyze the energy landscape $E(x,y)$ as the circular domain Σ grows. As the domain radius increases beyond $R_*=4\kappa/\lambda$, the minimum at (0,0) becomes higher than the energy at (1,0). As the domain radius increases to $R_+=8\kappa/\lambda$, the barrier between (0,0) and (1,0) disappears entirely. However, if $\epsilon>16\kappa^2\mu/\lambda^2$, the point (1,0) is not a local minimum, with an energy already higher than the minimum at (1,1). So if budding is induced at the radius R_+, then the ESCRTs either stay on the bud, if $\epsilon<16\kappa^2\mu/\lambda^2$, or they coalesce into the neck immediately after bud formation if $\epsilon>16\kappa^2\mu/\lambda^2$.

Another budding scenario is possible if $\epsilon>2\kappa$ and $\sqrt{A/\pi}<4\epsilon/\lambda$. The system evolves then on energy surface E_{II} from point (0,0) to (1,0) with no energy barriers, which means that flat, ESCRT-coated membrane domains are unstable and small, ESCRT-free buds with radius $R_b\to 0$ form spontaneously. The mini-buds induced by a strong binding preference ϵ to membrane portions with negative Gaussian curvature are next squeezed bigger by line tension if $\lambda>\mu\sqrt{A/\pi}$. The system evolves then from point (1,0) to (1,1). The resulting ESCRT-free buds have a radius $R_b<\lambda/2\mu$. In contrast to the three-stage mechanism, in this budding pathway the ESCRTs never enter the bud lumen.

Acknowledgments

We thank Dr. Thomas Wollert for stimulating discussions.

Author Contributions

Conceived and designed the experiments: BR EB JHH GH. Performed the experiments: BR. Analyzed the data: BR EB JHH GH. Contributed reagents/materials/analysis tools: BR GH. Wrote the paper: BR EB JHH GH.

References

1. Peter BJ, Kent HM, Mills IG, Vallis Y, Butler PJG, et al. (2004) BAR domains as sensors of membrane curvature: The amphiphysin BAR structure. Science 303: 495–499.
2. Brodsky FM, Chen CY, Knuehl C, Towler MC, Wakeham DE (2001) Biological basket weaving: Formation and function of clathrin-coated vesicles. Annu Rev Cell Dev Biol 17: 517–568.
3. Zimmerberg J, Kozlov MM (2006) How proteins produce cellular membrane curvature. Nature Rev Mol Cell Biol 7: 9–19.
4. Arkhipov A, Yin Y, Schulten K (2008) Four-scale description of membrane sculpting by BAR domains. Biophys J 95: 2806–2821.
5. Blood PD, Swenson RD, Voth GA (2008) Factors inuencing local membrane curvature induction by N-BAR domains as revealed by molecular dynamics simulations. Biophys J 95: 1866–1876.
6. Gruenberg J, Stenmark H (2004) The biogenesis of multivesicular endosomes. Nature Rev Mol Cell Biol 5: 317–323.
7. Piper RC, Katzmann DJ (2007) Biogenesis and function of multivesicular bodies. Annu Rev Cell Dev Biol 23: 519–547.
8. Hurley JH (2008) ESCRT complexes and the biogenesis of multivesicular bodies. Curr Opin Cell Biol 20: 4–11.
9. Raiborg C, Stenmark H (2009) The ESCRT machinery in endosomal sorting of ubiquitylated membrane proteins. Nature 458: 445–452.
10. Hanson PI, Shim S, Merrill SA (2009) Cell biology of the ESCRT machinery. Curr Opin Cell Biol 21: 568–574.
11. Babst M, Wendland B, Estepa EJ, Emr SD (1998) The Vps4p AAA ATPase regulates membrane association of a Vps protein complex required for normal endosome function. EMBO J 17: 2982–2993.
12. Wollert T, Wunder C, Lippincott-Schwartz J, Hurley JH (2009) Membrane scission by the ESCRT-III complex. Nature 458: 172–178.
13. Wollert T, Hurley JH (2010) Molecular mechanism of multivesicular body biogenesis by ESCRT complexes. Nature 464: 864–870.
14. Saksena S,Wahlman J, Teis D, Johnson AE, Emr SD (2009) Snapshot: The ESCRT machinery. Cell 137: 182.e1.
15. Hanson PI, Roth R, Lin Y, Heuser JE (2008) Plasma membrane deformation by circular arrays of ESCRT-III protein filaments. J Cell Biol 180: 389–402.
16. Lenz M, Crow DJG, Joanny JF (2009) Membrane buckling induced by curved filaments. Phys Rev Lett 103: 038101.
17. Hurley J, Boura E, Carlson LA, Rozycki B (2010) Membrane budding. Cell 143: 875–887.
18. Babst M (2011) MVB vesicle formation: ESCRT-dependent, ESCRT-independent and everything in between. Curr Opin Cell Biol 23: 452–457.
19. Fabrikant G, Lata S, Riches JD, Briggs JAG, Weissenhorn W, et al. (2009) Computational model of membrane fission catalyzed by ESCRT-III. PLoS Comput Biol 5: e1000575.
20. Murk JLAN, Humbel BM, Ziese U, Griffith J, Posthuma G, et al. (2003) Endosomal compartmentalization in three dimensions: Implications for membrane fusion. Proc Natl Acad Sci U S A 100: 13332–13337.
21. Boura E, Ivanov V, Carlson LA, Mizuuchi K, Hurley JH (2012) Endosomal Sorting Complex Required for Transport (ESCRT) complexes induce phase-separated microdomains in supported lipid bilayers. J Biol Chem 287: 28144–28151.
22. Helfrich W (1973) Elastic properties of lipid membranes - theory and possible experiments. Z Naturforsch 28c: 693–703.
23. Lipowsky R (1991) The conformation of membranes. Nature 349: 475–481.
24. Frolov VA, Lizunov VA, Dunina-Barkovskaya AY, Samsonov AV, Zimmerberg J (2003) Shape bistability of a membrane neck: A toggle switch to control vesicle content release. Proc Natl Acad Sci U S A 100: 8698–8703.
25. Kozlovsky Y, Kozlov MM (2003) Membrane fission: Theoretical model. Biophys J 84: 193A–193A.
26. Shibata Y, Hu JJ, Kozlov MM, Rapoport TA (2009) Mechanisms shaping the membranes of cellular organelles. Annu Rev Cell Dev Biol 25: 329–354.
27. Auth T, Gompper G (2009) Budding and vesiculation induced by conical membrane inclusions. Phys Rev E 80: 031901.
28. Bassereau P (2010) Division of labour in ESCRT complexes. Nature Cell Biol 12: 422–423.

29. Rossman J, Jing X, Leser G, Lamb R (2010) Inuenza virus M2 protein mediates ESCRT-independent membrane scission. Cell 142: 902–913.
30. Schmidt N, Mishra A, Lai G, Davis M, Sanders L, et al. (2011) Criterion for amino acid composition of defensins and antimicrobial peptides based on geometry of membrane destabilization. J Am Chem Soc 133: 6720–6727.
31. Braun A, Sevcsik E, Chin P, Rhoades E, Tristram-Nagle S, et al. (2012) α-synuclein induces both positive mean curvature and negative gaussian curvature in membranes. J Am Chem Soc 134: 2613–2620.
32. Kostelansky MS, Schluter C, Tam YYC, Lee S, Ghirlando R, et al. (2007) Molecular architecture and functional model of the complete yeast ESCRT-I heterotetramer. Cell 129: 485–498.
33. Im YJ, Hurley JH (2008) Integrated structural model and membrane targeting mechanism of the human ESCRT-II complex. Dev Cell 14: 902–913.
34. Sobo K, Chevallier J, Parton R, Gruenberg J, van der Goot F (2007) Diversity of raft-like domains in late endosomes. PLoS ONE 2: e391.
35. Möbius W, van Donselaar E, Ohno-Iwashita Y, Shimada Y, Heijnen HFG, et al. (2003) Recycling compartments and the internal vesicles of multivesicular bodies harbor most of the cholesterol found in the endocytic pathway. Traffic 4: 222–231.
36. Möbius W, Ohno-Iwashita Y, van Donselaar EG, Oorschot VMJ, Shimada Y, et al. (2002) Immunoelectron microscopic localization of cholesterol using biotinylated and non-cytolytic perfringolysin O. J Histochem Cytochem 50: 43–55.
37. Sorre B, Callan-Jones A, Manneville JB, Nassoy P, Joanny JF, et al. (2009) Curvature-driven lipid sorting needs proximity to a demixing point and is aided by proteins. Proc Natl Acad Sci U S A 106: 5622–5626.
38. Mbamala EC, Ben-Shaul A, May S (2005) Domain formation induced by the adsorption of charged proteins on mixed lipid membranes. Biophys J 88: 1702–1714.
39. Heimburg T, Angerstein B, Marsh D (1999) Binding of peripheral proteins to mixed lipid membranes: Effect of lipid demixing upon binding. Biophys J 76: 2575–2586.
40. van den Bogaart G, Meyenberg K, Risselada HJ, Amin H, Willig KI, et al. (2011) Membrane protein sequestering by ionic protein-lipid interactions. Nature 479: 552–555.
41. Liu J, Kaksonen M, Drubin DG, Oster G (2006) Endocytic vesicle scission by lipid phase boundary forces. Proc Natl Acad Sci U S A 103: 10277–10282.
42. Honerkamp-Smith AR, Cicuta P, Collins MD, Veatch SL, den Nijs M, et al. (2008) Line tensions, correlation lengths, and critical exponents in lipid membranes near critical points. Biophys J 95: 236–246.
43. Ayton GS, McWhirter JL, McMurtry P, Voth GA (2008) Coupling field theory with continuum mechanics: A simulation of domain formation in giant unilamellar vesicles. Biophys J 88: 3855–3869.
44. Garcia-Saez AJ, Schwille P (2008) Stability of lipid domains. FEBS Lett 584: 1653–1658.
45. Lipowsky R (1992) Budding of membranes induced by intramembrane domains. J Phys II 2: 1825–1840.
46. Jülicher F, Lipowsky R (1993) Domain-induced budding of vesicles. Phys Rev Lett 70: 2964–2967.
47. Baumgart T, Hess S, Webb WW (2003) Imaging coexisting uid domains in biomembrane models coupling curvature and line tension. Nature 425: 821–824.
48. Yanagisawa M, Imai M, Taniguchi T (2008) Shape deformation of ternary vesicles coupled with phase separation. Phys Rev Lett 100: 148102.
49. Sens P, Turner MS (2006) Budded membrane microdomains as tension regulators. Phys Rev E 73: 031918.
50. Boura E, Różycki B, Chung H, Herrick D, Canagarajah B, et al. (2012) Solution structure of the ESCRT-I and -II supercomplex: implications for membrane budding and scission. Structure 20: 874–886.
51. Ramadurai S, Holt A, Krasnikov V, van den Bogaart G, Killian JA, et al. (2009) Lateral diffusion of membrane proteins. J Am Chem Soc 131: 12650–12656.
52. Nickerson D, West M, Henry R, Odorizzi G (2010) Regulators of Vps4 ATPase activity at endosomes di_erentially inuence the size and rate of formation of intralumenal vesicles. Mol Biol Cell 21: 1023–1032.
53. Wilhelm C, Cebers A, Bacri JC, Gazeau F (2003) Deformation of intracellular endosomes under a magnetic field. Eur Biophys J 32: 655–660.
54. Roux A, Cuvelier D, Nassoy P, Prost J, Bassereau P, et al. (2005) Role of curvature and phase transition in lipid sorting and fission of membrane tubules. EMBO J 24: 1537–1545.
55. Settles E, Loftus A, McKeown A, Parthasarathy R (2010) The vesicle trafficking protein Sar1 lowers lipid membrane rigidity. Biophys J 99: 1539–1545.
56. Shchelokovskyy P, Tristram-Nagle S, Dimova R (2011) Effect of the HIV-1 fusion peptide on the mechanical properties and leaet coupling of lipid bilayers. New J Phys 13: 025004.
57. Siegel D (2008) The gaussian curvature elastic energy of intermediates in membrane fusion. Biophys J 95: 52005215.
58. Siegel D, Kozlov M (2004) The gaussian curvature elastic modulus of nmonomethylated dioleoylphosphatidylethanolamine: Relevance to membrane fusion and lipid phase behavior. Biophys J 87: 366–374.
59. Boura E, Różycki B, Herrick D, Chung H, Vecer J, et al. (2011) Solution structure of the ESCRT-I complex by small-angle X-ray scattering, EPR, and FRET spectroscopy. Proc Natl Acad Sci U S A 108: 9437–9442.
60. Jülicher F, Seifert U (1994) Shape equations for axisymmetrical vesicles - a clarifi- cation. Phys Rev E 49: 4728–4731.
61. Jülicher F, Lipowsky R (1996) Shape transformations of inhomogeneous vesicles with intramembrane domains. Phys Rev E 53: 2670–2683.
62. Góźdź W (2007) Deformations of lipid vesicles induced by attached spherical particles. Langmuir 23: 5665–5669.
63. Góźdź WT (2005) Inuence of spontaneous curvature and microtubules on the conformations of lipid vesicles. J Phys Chem B 109: 21145–21149.